Article:
Rees-Zimmerman, C.R., Chan, D.H.H., Armes, S.P. orcid.org/0000-0002-8289-6351 et al. (1 more author) (2023) Diffusiophoresis of latex driven by anionic nanoparticles and their counterions. Journal of Colloid and Interface Science, 649. pp. 364-371. ISSN 0021-9797

https://doi.org/10.1016/j.jcis.2023.06.115

Journal of Colloid and Interface Science 649 (2023) 364–371

Contents lists available at ScienceDirect

Journal of Colloid And Interface Science

journal homepage: www.elsevier.com/locate/jcis

Diffusiophoresis of latex driven by anionic nanoparticles and their counterions

Clare R. Rees-Zimmerman [a,1], Derek H.H. Chan [b], Steven P. Armes [b], Alexander F. Routh [a,*]

[a] Institute of Energy and Environmental Flows, Department of Chemical Engineering & Biotechnology, University of Cambridge, Madingley Rise, Cambridge CB3 0EZ, UK
[b] Dainton Building, Department of Chemistry, University of Sheffield, Brook Hill, Sheffield S3 7HF, UK

GRAPHICAL ABSTRACT

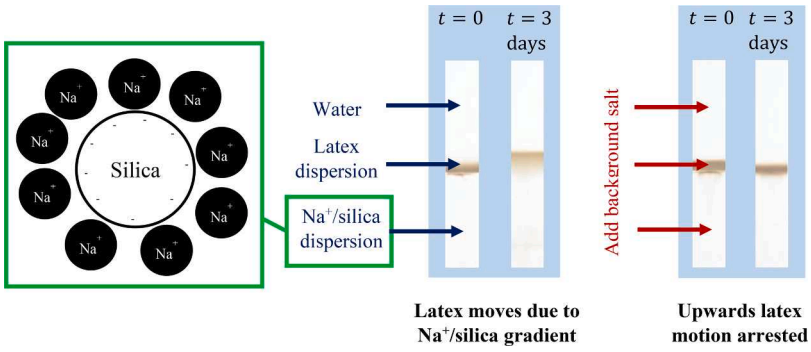

ARTICLE INFO

Keywords:
Colloidal hydrodynamics
Diffusiophoresis
Multivalent electrolytes
Silica nanoparticles
Diblock copolymer nanoparticles
Hele-Shaw cell

ABSTRACT

Hypothesis: Diffusiophoresis of colloidal latex particles has been reported for molecular anions and cations of comparable size. In the present study, this phenomenon is observed for two types of charged colloids acting as multivalent electrolyte: (i) anionic charge-stabilised silica nanoparticles or (ii) minimally-charged sterically-stabilised diblock copolymer nanoparticles.

Experiments: Using a Hele-Shaw cell, a thin layer of relatively large latex particles is established within a sharp concentration gradient of nanoparticles by sequential filling with water, latex particles and nanoparticles. Asymmetric diffusion is observed, which provides strong evidence for diffusiophoresis. Quantification involves turbidity measurements from backlit images.

Findings: The latex particles diffuse across a concentration gradient of charged nanoparticles and the latex concentration front scales approximately with time$^{1/2}$. Moreover, the latex particle flux is inversely proportional to the concentration of background salt, confirming electrostatically-driven motion. These observations are consistent with theory recently developed to account for diffusiophoretic motion driven by multivalent ions.

Abbreviations: CPDB, 2-cyano-2-propyl benzodithioate; PGMA, poly(glycerol monomethacrylate); PTFEMA, poly(2,2,2-trifluoroethyl methacrylate).

* Corresponding author.
E-mail address: afr10@cam.ac.uk (A.F. Routh).
[1] Present address: Department of Chemistry, Physical and Theoretical Chemistry Laboratory, University of Oxford, South Parks Road, Oxford OX1 3QZ, UK.

https://doi.org/10.1016/j.jcis.2023.06.115
Received 5 May 2023; Received in revised form 12 June 2023; Accepted 16 June 2023
Available online 17 June 2023

1. Introduction

Diffusiophoresis is the motion of colloidal particles or small molecules across a concentration gradient comprising a suitable solute. In principle, it can involve electrolytes or non-electrolytes, and may result in motion either up or down the solute concentration gradient [1]. Fig. 1 illustrates the difference between diffusion and diffusiophoresis. Herein we investigate electrolyte-driven diffusiophoresis, which involves both electrophoresis and chemiphoresis [2]. In an electrolyte gradient, differing diffusivities for the cations and anions result in an electric field, which drives the electrophoretic motion of a charged colloidal particle. Moreover, this electric field produces a pressure gradient within the electrical double layer of such particles owing to electrolyte adsorption, which drives fluid flow along the colloid surface. The resulting chemiphoresis always results in motion of the colloidal particles up the ion concentration gradient. In contrast, electrophoresis can result in motion in either direction, depending on the particle charge and the differing ion diffusivities [3]. Such diffusiophoretic motion can be exploited to enhance particle motion within microchannels for lab-on-a-chip devices [4] or to control particle motion in drying films [5].

Electrolyte-driven diffusiophoresis has been studied extensively for electrolytes containing ions of the same valency. For example, Ebel *et al.* [6] examined the diffusiophoresis of latex particles across a porous membrane separating electrolyte solutions (e.g. KCl or NaCl) of differing concentration. Recently, Wilson *et al.* [7] conducted diffusiophoresis experiments using fluorescent latex particles and multivalent electrolytes (e.g. $CaCl_2$ or Na_2SO_4). In this case, latex diffusion was negligible compared to the diffusiophoretic motion. The latter phenomenon was governed by the ambipolar diffusivity, D_a, which is related to the ion diffusion coefficients.

Colloidal particles are typically either charge or sterically stabilised [8,9]. So-called electrosteric stabilisation, which combines both mechanisms, is also known [10]. Aqueous dispersions of charge-stabilised nanoparticles typically contain much smaller counterions [11,12]. However, to the best of our knowledge no-one has yet explored whether such charge-stabilised nanoparticles, which could be considered as multivalent electrolytes, promote diffusiophoresis.

Diffusiophoresis is typically investigated for geometries with no net convective flux, such as dead-end channels [13], microfluidic devices [14], or Hele-Shaw cells [15]. A Hele-Shaw cell comprises a pair of parallel plates separated by a narrow gap and is used for studying laminar flow [16]. Gravitational settling is often studied using vertically-oriented Hele-Shaw cells [17], whereas horizontally-oriented cells enable examination of viscous fingering [18]. The former setup is used herein to exploit the density difference between the latex and nanoparticles [8,19]. At this length scale, turbidity can be used to infer latex concentration [20], which avoids using relatively expensive fluorescent latex particles. Salt-driven diffusiophoresis experiments typically produce an initially sharp electrolyte gradient and the latex concentration profile is subsequently monitored over time [13,14].

In the present study, the nanoparticles act as multivalent anions that are much larger – and possess much higher charge – than the corresponding cations. Our primary objective is to characterise electrolyte-driven diffusiophoresis for such colloidal dispersions.

The first system involves diffusiophoresis of relatively large latex particles in the presence of sodium-stabilised silica nanoparticles. Both components are readily available and widely used for various industrial applications: silica nanoparticles are utilised in coatings, gels and catalysts [11] while latexes are employed for paints and coatings, adhesives and the manufacture of disposable gloves [21]. Diffusiophoresis is exploited in certain applications, for example, for the deposition of latex paint onto steel [22]. Unfortunately, silica nanoparticles tend to form fractal agglomerates [23], which makes quantitative comparison with theory somewhat problematic. Thus, we also study the diffusiophoresis of latex in the presence of sterically-stabilised diblock copolymer nanoparticles. Such nanoparticles comprise a hydrophobic poly(2,2,2-trifluoroethyl methacrylate) (PTFEMA) core-forming block and a hydrophilic poly(glycerol monomethacrylate) (PGMA) stabiliser block, which bears either an ionisable carboxylic acid end-group or a permanently non-ionic end-group (see Fig. A.1 in Appendix A.1). The HOOC-PGMA-PTFEMA nanoparticles offer two important advantages over the silica nanoparticles: (i) they do not suffer from incipient aggregation and (ii) their minimal surface charge (just one anionic charge per copolymer chain at an appropriate solution pH) means that the number of charges per nanoparticle, z_-, is intimately linked to the mean number of copolymer chains per nanoparticle, which can be conveniently adjusted by varying the appropriate synthesis parameters (i.e. the mean degree of polymerisation of the PGMA and PTFEMA blocks, respectively).

The motion of latex particles within a nanoparticle/counterion concentration gradient is both modelled and tracked experimentally. Our methodology – both experiment design and the selection of suitable colloidal dispersions – is presented in Section 2. The results are presented and discussed in Section 3. Predictions using existing theory for multivalent electrolyte diffusiophoresis are presented in Section 4, and conclusions are drawn in Section 5.

2. Material and methods

2.1. Experimental design

A dead-end channel was chosen to ensure that there is no net convective flux. This is important given the relatively long timescale required for diffusion: the particles should not experience any convection during the experiment, other than due to diffusioosmotic wall slip, which we estimate to negligibly affect the motion of the latex particles [24]. This is calculated in Appendix C.2.3. Our Hele-Shaw cell setup

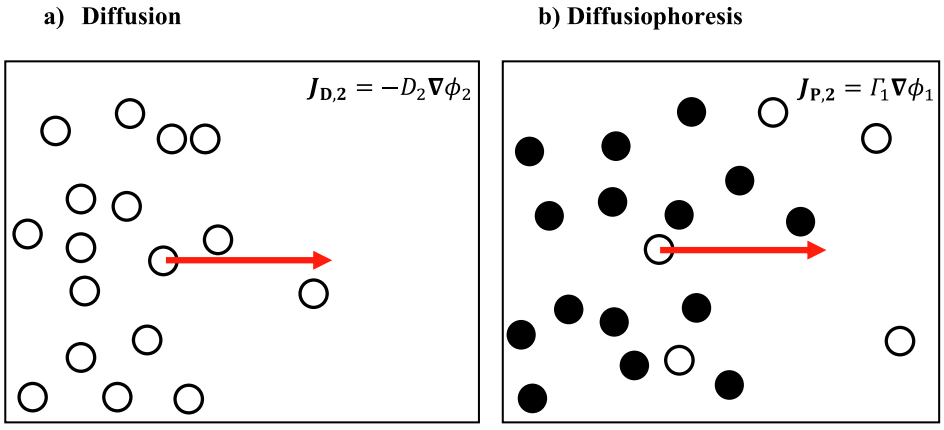

Fig. 1. Illustration of diffusive and diffusiophoretic motion. **a)** Diffusive motion (subscript D). Equations for the flux of component two, J_2, are given for dilute solution. **b)** Diffusiophoretic motion (subscript P). The net flux, depicted by the red arrow, of component two particles (open circles) could be either up or down the concentration gradient imposed by the component one particles (filled circles), depending on the sign of the diffusiophoretic drift coefficient, Γ_1. The volume fraction of each component is denoted by ϕ. (For interpretation of the references to colour in this figure legend, the reader is referred to the web version of this article.)

resembles the dead-end microfluidic channels employed to study diffusiophoresis in the literature [13], albeit on a longer length scale. The internal cell dimensions are approximately 3 mm (depth) by 2 cm (width) by 20 cm (height). A 3 mm distance between the acrylic plates was chosen because surface imperfections may become visible for narrower gaps. By filling the tank with dye using a microfluidic syringe pump at a known flow rate, and recording the increase in height for the dyed water over time, the inter-plate gap is estimated to be 3.15 ± 0.05 mm. The choice of a 2 cm width is a trade-off between minimising the time required to fill the tank when using a relatively slow flow rate versus the need to provide sufficient width for image analysis to ensure that edge effects are negligible. The choice of a 20 cm height was somewhat arbitrary but sufficient distance is required to observe the particle motion.

With this method, only the latex motion can be tracked, since the silica particles are not visible to the camera. It is typical of salt-driven diffusiophoresis studies to not track the ions driving the diffusiophoresis, only the particles undergoing the diffusiophoresis [7,13,14] – though understandably, in salt-driven diffusiophoresis studies, ions of atomic size would be difficult to track. A more expensive and difficult experiment, not possible with the current setup, would be required to also track the silica particles. For example, fluorescent particles could be used in place of both the silica and the latex particles, with filters for the camera. Fluorescent particles would be significantly more expensive, and so require using a microfluidic set-up, rather than a Hele-Shaw cell, to reduce the volume required. Therefore, this study focusses on the most interesting motion – the latex particles undergoing diffusiophoresis.

2.2. Experiment set-up

A sharp concentration gradient comprising either silica or PGMA-PTFEMA nanoparticles is set up by filling the tank sequentially with three layers (Fig. 2b): deionized water (Milli-Q Direct 8 Water Purification System, 18.2 MΩ-cm ultrapure water output), a thin middle layer of latex particles, and a final lower layer of nanoparticles. The particle diameters, d_n, obtained using dynamic light scattering (DLS) are 24 nm & 27 nm for the HOOC-PGMA-PTFEMA & CPDB-PGMA-PTFEMA nanoparticles, and 103, 155, or 242 nm for the latex. Based on their specific surface area, the three silica sols have nominal diameters of 7, 12 or 22 nm. Filling the tank with three layers is straightforward and also ensures a suitable timescale for the subsequent latex motion. The timescale for detectable motion of the latex front scales as the resolution, r, of the imaging set-up divided by the diffusiophoretic velocity, U_E. The total height of fluid is L, and the interface between the latex and nanoparticle layers occurs at a height x_0.

The tank is filled from the bottom using two syringe pumps, which are connected to the single inlet at the base of the tank. Filling the tank in order of increasing fluid density produces suitably stratified layers [25]. One syringe pumps the aqueous dispersion of latex particles, while the other pumps the aqueous dispersion of nanoparticles. First, both fluids are pumped at a flow rate of 0.8 ml min^{-1} in order to displace any air bubbles. The waste fluid is then allowed to drain by disconnecting the inlet, and any remaining latex/nanoparticles are removed by injecting deionized water from the top of the tank using a syringe equipped with a long needle. The latex layer is created by pumping an aqueous latex dispersion into the tank at a flow rate of 0.2 ml min^{-1}. As the latex dispersion reaches the tank entrance, its flow is stopped, and the water layer is created by injecting deionized water from the top of the tank. Finally, the nanoparticle dispersion is pumped into the tank at a flow rate of 0.2 ml min^{-1}, until the latex layer has reached the desired height. The inlet at the base of the tank is rectangular (1.6×3 mm). Thus this flow rate corresponds to a Reynolds number of 1.4, which is deemed to be sufficiently low.

In subsequent experiments, the deionized water is replaced with various salt solutions (Section 3.2), and the same salt concentration is also present within the aqueous latex and nanoparticle layers. Experiments are also conducted with latexes and silica sols of differing size (Appendix D.2), and at a 45° angle (Appendix D.3).

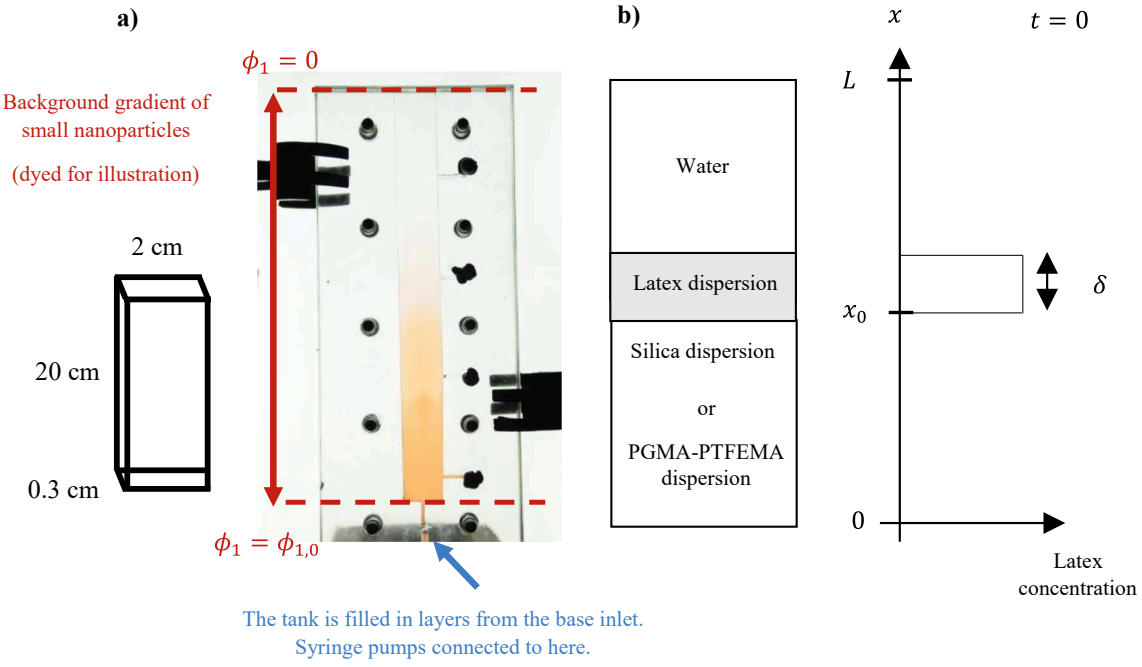

Fig. 2. Hele-Shaw cell experimental set-up. **a)** A digital photograph of the tank in which the aqueous silica dispersion has been dyed for illustration. The upper layer comprises deionized water, and there is no latex layer present in this example. Inset: dimensions of the tank channel. **b)** Schematic representation of the diffusiophoresis experiment, showing (left) the initial layering of the fluids in the tank, and (right) the intended initial latex concentration condition, which is the variable inferred in the experiment.

2.3. Materials

Three silica sols SM30, HS40 and TM40 were sourced from Sigma-Aldrich, and their hydrodynamic diameters were around 30 nm as determined by DLS (Brookhaven Nanobrook Omni). PGMA-PTFEMA synthesis and characterization details are given in Appendix A.1.

The silica and PGMA-PTFEMA nanoparticles were dialyzed against deionized water to remove salts and hence ensure that each dispersion comprised just the nanoparticles and their respective counterions (i.e., Na^+/silica or $H^+/^-$OOC-PGMA-PTFEMA nanoparticles), to maintain electroneutrality. After dialysis and dilution, these aqueous dispersions had a density of 1.09 g cm^{-3} and contained either ~ 5 vol% (PGMA-PTFEMA) or ~ 6 vol% (silica) nanoparticles. Full details of silica dispersion densities, particle sizes and zeta potentials are provided in Appendix A.2. These data are used to estimate the mean number of charges per silica nanoparticle, z_-.

The latex particles comprised a methyl methacrylate-butyl acrylate-acrylic acid (PMMA-BA) copolymer, prepared via aqueous emulsion copolymerisation, using a potassium persulfate initiator [26] which results in the latex particles' negative zeta potential. The hydrodynamic diameters and zeta potentials for the three latexes used in this study are summarised in Appendix A.3.

Appendix A.4 summarizes solution conductivities for the latexes and silica sols, which increase linearly with added salt concentration. The data provided in Appendix A.5 confirms that each dispersion remained colloidally stable under the conditions employed in these experiments.

3. Results and discussion

3.1. Comparison of test and control experiments

Fig. 3 shows representative images recorded for the Hele-Shaw cell

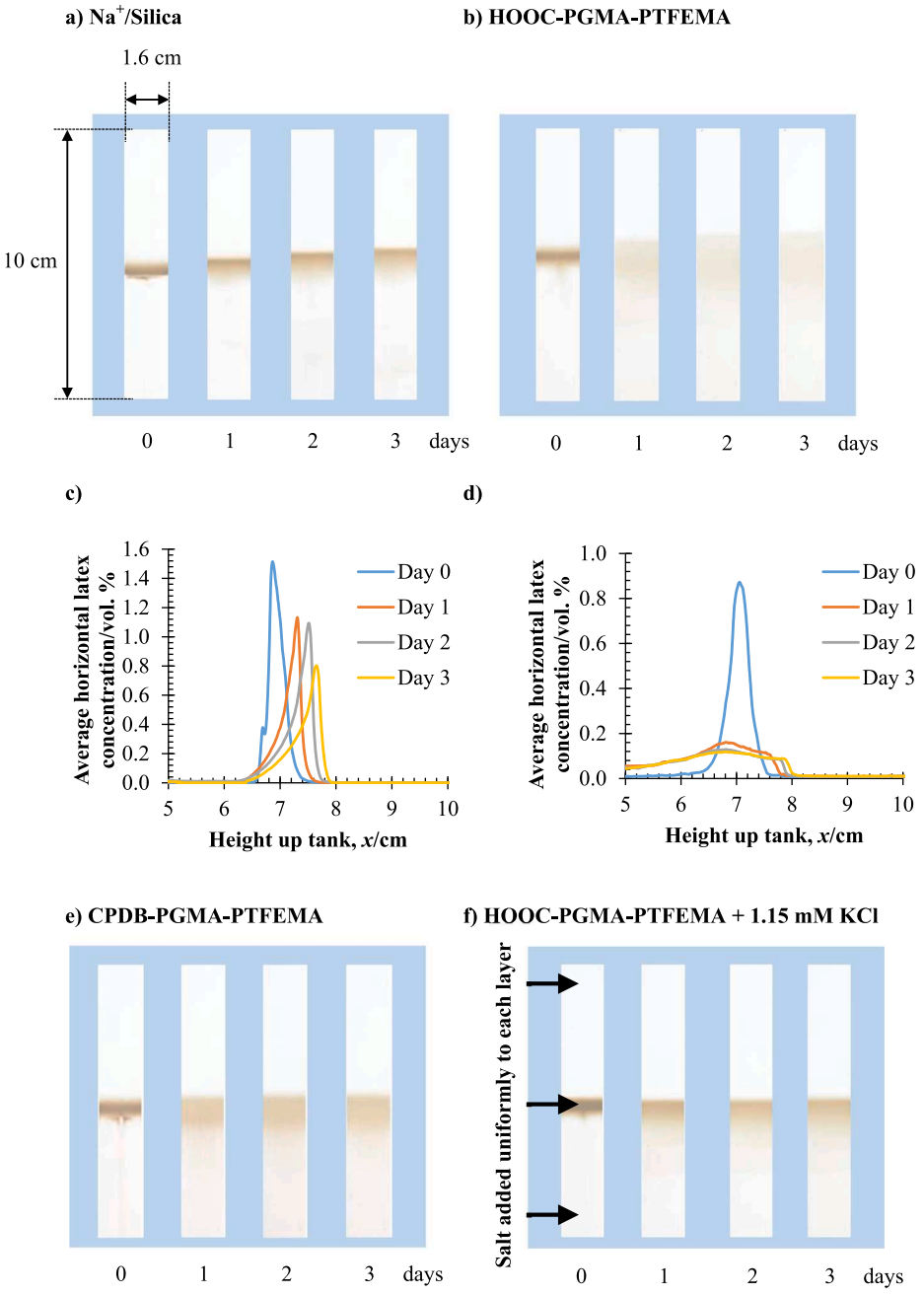

Fig. 3. Representative time lapses of the motion of latex particles in nanoparticle concentration gradients. These were obtained from images recorded for Hele-Shaw cell experiments conducted using **a)** Na^+/silica and **b)** $H^+/^-$OOC-PGMA-PTFEMA nanoparticles, as outlined in Fig. 2, for the case where latex $d_{n,2} = 155$ nm, and their corresponding conversions to horizontally-averaged latex concentration profiles in **c)** and **d)**, respectively. In a), $d_{n,1} = 12$ nm and the solution density of the silica dispersion is 1.09 g cm^{-3}. Control experiment time lapses are shown in **e)**, for non-ionic CPDB-PGMA-PTFEMA nanoparticles, and **f)**, for $H^+/^-$OOC-PGMA-PTFEMA nanoparticles in which 1.15 mM KCl is added to each layer at the start of the experiment. In b), e) & f), the nanoparticle dispersion density is 1.01 g cm^{-3}, and $d_{n,1} = 24$ nm (b & f) or 27 nm (e). Images a), b), e) & f) have the same scale.

over time for the diffusiophoresis (Na^+/silica; HOOC-PGMA-PTFEMA) and control (CPDB-PGMA-PTFEMA) experiments conducted using the 155 nm latex. It takes 30 min to pump in the nanoparticle layer, such that the latex layer is located in the middle of the tank. This time is negligible compared to the timescale of the experiment. Once the latex layer has reached its final height, this time is taken to be zero time or "day 0". Inspecting Fig. 3a, the latex boundary moves upwards against gravity over 72 h. Some sedimentation is discernible in Fig. 3b, but the upper latex front continues to move upwards, which indicates diffusiophoresis.

Quantification of the motion involves determination of turbidity by analysis of backlit images of the flow cell. Details of the calibration are given in Appendix B. The diffusiophoresis images obtained for each experiment were analysed by using each pixel's calibration curve (Fig. B.1b in Appendix B) to convert the pixel reading into a latex concentration. Example concentration profiles for Fig. 3a & b are shown in Fig. 3c & d. In Fig. 3c, the concentration profile is initially approximately symmetric (day 0) and centred at a height x of 7 cm. Unlike the idealised sketch shown in Fig. 2b, there is typically some overlap between the central latex layer and those layers above and below: the initial concentration profile resembles a Gaussian distribution, with a standard deviation of ~0.14 cm. The peak position moves upwards, rising 0.78 cm over three days, while the peak concentration progressively decreases as the profile widens. The profile becomes increasingly negatively skewed: a sharp latex dispersion/water boundary is formed at the top of the latex dispersion layer. This indicates that minimal sedimentation occurs within the three-day time scale of this experiment. Fig. 3e shows data for the control experiment. In this case, the non-ionic CPDB-PGMA-PTFEMA nanoparticles possess no charged end-groups, and hence no associated counterions, so there is minimal upwards latex motion. An additional control experiment containing only latex and water is presented in Appendix D.1.

The absolute concentrations are subject to some experimental error, particularly at the higher concentrations as the calibration curve starts to flatten (Fig. B.1b in Appendix B). Nevertheless, identification of the peak position should be accurate. The spatial resolution for the images shown in these examples is 221 pixels cm^{-1}.

3.2. *Effect of varying conductivity*

To confirm that the observed upwards motion of the latex front is electrostatically-driven – and to examine the theoretical prediction that $U_E = D_E \nabla \ln c_{s,total}$ (equation (C.1.4), Appendix C.1) – the diffusiophoresis experiments (Fig. 3a & b) are repeated with salt added to all three layers

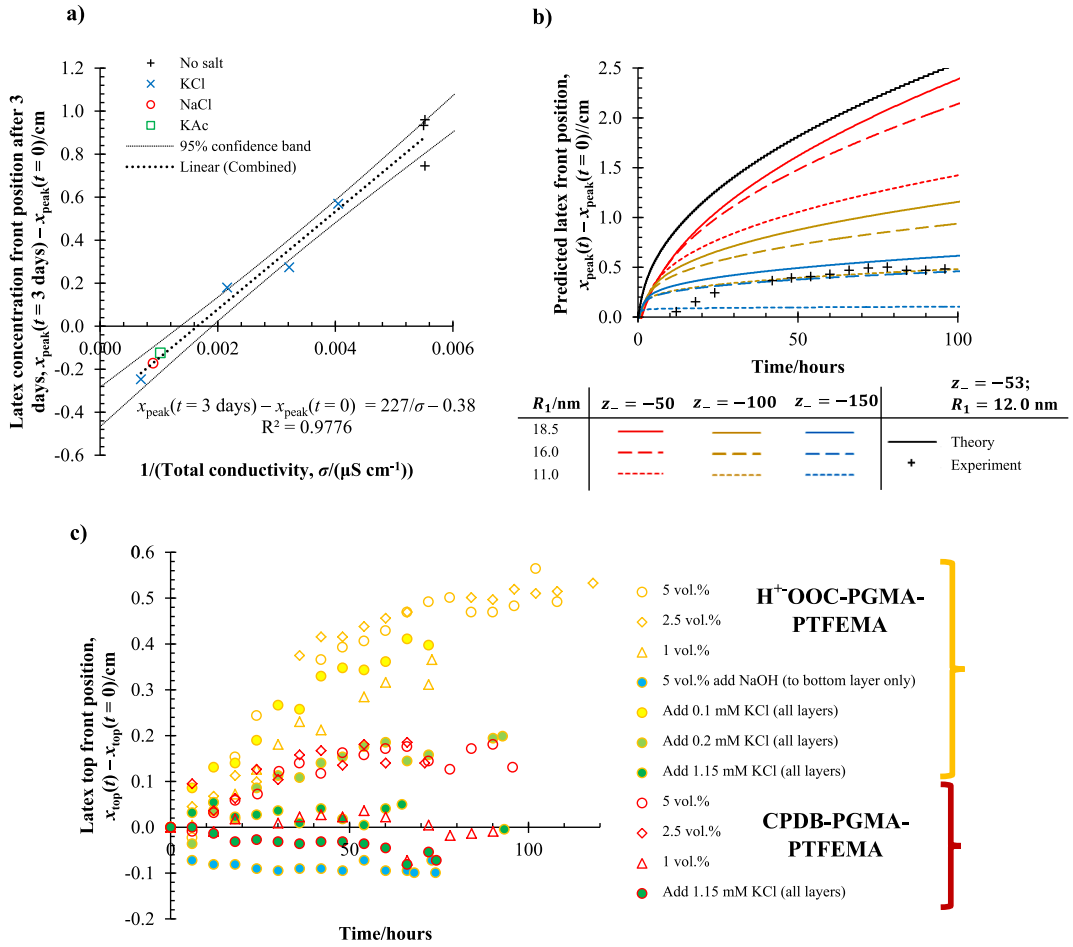

Fig. 4. Trajectories of diffusiophoretic latex motion in nanoparticle concentration gradients. **a)** Plot of the latex concentration front position observed after three days against the reciprocal of the conductivity of the latex dispersion for the silica experiments shown in Fig. 3a but in the presence of various added salts. A linear regression fit to all the data points is shown, along with its 95% confidence band. Based on image/calibration resolution and conductivity meter precision, the error bars for these data points are too small to be discernible. **b)** Plot of the position of the latex concentration front as a function of time for **(1)** the case shown in Fig. 3a – theoretical predictions are shown for a range of R_1 and z_- values (assuming a spherical morphology for the silica nanoparticles) – and **(2)** the HOOC-PGMA-PTFEMA nanoparticle experiment shown in Fig. 3b (predicted and experimental values indicated by the black line and black crosses, respectively). The theoretical predictions correspond to the case with negligible added salt. **c)** Plot of the position of the horizontally averaged peak latex concentration as a function of time for the cases shown in Fig. 3b & 3e over a range of PGMA-PTFEMA nanoparticle concentrations (Fig. 3b after adjusting the solution pH with NaOH and Fig. 3f conducted with a series of KCl concentrations).

(nanoparticle dispersion, latex dispersion, and water). The diffusiophoretic mobility of the latex is denoted by D_E, and the total salt concentration by $c_{s,total}$. There is no salt concentration gradient, so this cannot drive diffusiophoresis. Instead, the added salt screens the electric field resulting from the nanoparticle/counterion motion [27]. Fig. 3f shows a series of time lapse photographs recorded for an experiment performed under the same conditions as that shown in Fig. 3b but with 1.15 mM KCl added to each of the three layers.

In contrast to Fig. 3b, a slight downwards motion of the latex front (-0.25 cm over three days) is observed. This suggests that the added salt has arrested motion arising from electrolyte-driven diffusiophoresis. The observed minimal apparent motion is attributed to partial sedimentation of the latex particles, with leakage and air bubbles also potentially making a contribution. The Na^+/silica experiment was conducted in the presence of 10 mM NaCl, 10 mM potassium acetate (KAc), and a series of KCl concentrations (0.575 mM, 1.15 mM, 2.50 mM and 10 mM). To enable direct comparison between salts with differing ion mobilities, the latex concentration front position is plotted against the reciprocal of the total conductivity of the initial latex dispersion in Fig. 4a. The silica/counter-ion concentration gradient is the same in each experiment, but the total salt concentration differs.

Repeats of the 'no added salt' experiment (Fig. 3a) are shown in Fig. 4a ('no salt') to demonstrate the reproducibility of such experiments. These experiments included different camera calibrations – a new calibration is required each time the camera/tank was moved – and various batches of dialysed silica dispersions and diluted latex dispersions. These technical issues are considered to have only a small effect on the data: the main contribution to experimental differences between runs is likely to be variations in the initial nanoparticle concentration profile arising from filling the tank.

The data indicate a linear relationship between the latex concentration front position and the reciprocal of the total conductivity. This suggests that U_E is proportional to $\nabla \ln c_{s,total}$. This relation holds regardless of the type of added salt: the data obtained for KCl, NaCl, and KAc fall on the same line. The intercept (plus its standard error) is -0.38 ± 0.05 cm, which is consistent with gravitational sedimentation of the 155 nm latex particles within three days.

In Fig. 4c, the latex top front position at a given time, $x_{top}(t)$, relative to its initial position, $x_{top}(t=0)$, is plotted for a series of experiments performed using the anionic HOOC-PGMA-PTFEMA nanoparticles. The yellow data set includes different nanoparticle concentrations; increasing the nanoparticle concentration increases the upwards latex motion, indicating that $U_E \propto \nabla \ln c_{s,total}$. Over longer time scales (>12 h), the evolution of peak position has an approximate $t^{1/2}$dependence. Initial rearrangement of the latex layer or transient flow during tank filling may account for the differing behaviour observed at early times. It is also important to recognize that diffusiophoretic theory does not predict a $t^{1/2}$ dependence but closely resembles this scaling relation; the top boundary condition prevents motion continuing along this trajectory when $U_E t \sim (L - x_0)$.

The corresponding control experiments conducted using the non-ionic CPDB-PGMA-PTFEMA nanoparticles (red data set) result in a significant reduction in the upwards latex motion because these neutral nanoparticles contain no counterions. Increasing the KCl concentration when using the anionic HOOC-PGMA-PTFEMA nanoparticles (filled yellow circles) also reduces the upwards motion, which is similar to the data shown in Fig. 4a. Adding NaOH to the HOOC-PGMA-PTFEMA nanoparticle layer to adjust the solution pH to 7.5 partially replaces H^+ with Na^+ (yellow circle filled in blue). Since Na^+ is a significantly larger ion than H^+, this reduces the predicted D_a value so the upwards latex motion is no longer observed. Even if there were any excess NaOH, the absolute OH^- concentration would be very small at pH 7.5 (maximum possible value $\sim 10^{-6.5} = 3.2 \times 10^{-7}$M). However, we note that a NaOH gradient would cause diffusiophoresis of latex particles *up* the NaOH gradient [28].

3.3. Estimation of velocity magnitudes for various alternative phenomena

Estimates of other potentially relevant velocities are given in Table 1. Where applicable, the 7 nm silica sol and 242 nm copolymer latex are used to create upper bounds. In each case, these estimated magnitudes are small compared to the observed upwards latex motion. In contrast, electrolyte-driven diffusiophoresis is sufficiently large to account for the experimental observation (Fig. 4b).

Another possible explanation is that the mutual diffusion of nanoparticle/water has been modelled since both the nanoparticle and latex dispersions are dilute. Water molecules, as the solvent, would fill the space left by the diffusing nanoparticles. In principle, this could lead to a rise in the latex concentration front. However, the maximum rise owing to such an effect can be estimated based on the difference between a step function in nanoparticles, and a uniform nanoparticle dispersion: $\phi_{1,t=0} x_0/2 \sim 0.25$ cm. Since the rise in the latex concentration front with no added salt (~ 1 cm) is significantly larger than this estimated value, backflow of solvent is highly unlikely to account for the experimental observation.

Dialysis is employed to remove ions other than the nanoparticles and their counterions. Further evidence that silica nanoparticles alone cause diffusiophoresis – as opposed to traces of other ions – is that the value of D_E for the latex particles is *positive* in the presence of salts such as Na_2SO_4 [7], which would lead to latex diffusiophoresis *against* the salt concentration gradient, contrary to that observed experimentally.

4. Theory

The theory of Wilson *et al.* [7] for diffusiophoresis in the presence of a multivalent electrolyte is applied in the limit $|z_-| \gg z_+$(where $z_+ = 1$), and $\psi_2 < 0$ to predict the latex motion. [N.B. The valence, z, for the cations and anions is denoted by the subscripts + and −, respectively, with $z_- < 0$ and $z_+ > 0$, and ψ_2 denotes the zeta potential of the latex particles.] The mathematical derivation is given in Appendix C: Appendix C.1 presents the theory of multivalent electrolyte diffusiophoresis in this limit and Appendix C.2 applies this theory to the experimental setup, first considering sedimentation (Appendix C.2.1) and then solving a partial differential equation (PDE) model (Appendix C.2.2).

Fig. 4b shows example solutions and their sensitivity to numerical values for z_- and R_1, with $\psi_2 = -53$ mV. The exact morphology of the fractal silica particles is unknown, so they are taken to be spherical to obtain a hydrodynamic diameter ($2R_1$) via DLS, then we allow this parameter to vary to examine the solution sensitivity. The predicted front position of the latex concentration, $x_{peak}(t)$, is plotted relative to its initial position, $x_{peak}(t=0)$. The initial volume fraction of the nanoparticle layer is 0.06 for silica experiments and 0.05 for the PGMA-PTFEMA experiments, and that of the latex layer is 0.01. In the silica experiments, the relative viscosity of the medium between the top and

Table 1
Estimates of velocity magnitudes for various alternative phenomena.

Phenomenon	Typical velocity/(mm day^{-1})
Experimental observation: 1 cm upwards over 3 days	+ 3.3
Diffusion of 242 nm latex	± 0.24
Excluded volume diffusiophoresis in 7 nm silica	+ 0.26
Sedimentation of 242 nm latex in water	− 0.15
Creaming of 242 nm latex in 1.16 g cm^{-3} silica dispersion	+ 0.34
Fall of top water surface (leakage/rise of air bubbles): 0.2 cm over 3 days	− 0.67

The magnitude of excluded volume-diffusiophoresis is estimated using the velocity $U = -(3\phi_1 k_B T/8\pi\eta R_1)\nabla \ln \phi_1$ for an infinite particle size ratio [5]. The magnitude of the diffusive motion is estimated using $x - x_0 \sim \sqrt{D_2 t}$, where D_2 is the Stokes-Einstein diffusion coefficient for the latex particles.

bottom of the tank is expected to be within $\eta_r = 1.0$ (water) and $\eta_r = 1.5$ (estimated for the dialysed HS40 silica nanoparticles). Thus we assume $\eta_r = 1.0$ and note that the viscosity difference across the tank does not significantly affect the predictions. Upwards motion of the latex concentration front position is predicted over time, *down* the concentration gradient of Na^+/silica nanoparticles. The magnitude of the motion is sensitive to the numerical value of z_- for a given R_1 value: as z_- becomes less negative, the magnitude of U_E increases because D_E becomes more negative.

Lowering R_1 increases D_a but reduces β (see Appendix C.1), which in turn suppresses the diffusiophoretic motion. Decreasing R_1 from 16 nm (TM40 silica) to 11 nm (HS40 silica) roughly halves the D_E/D_a ratio and correspondingly affects the predicted motion of the latex front position. Although differing z_- values are estimated for each of the three silica dispersions (Table C.1, Appendix C.1), this is largely attributed to their differing hydrodynamic radii. The relationship between R_1 and z_- means that the effect of increasing z_- can be counteracted simply by choosing larger silica nanoparticles. If silica nanoparticles are assumed to have the same surface charge density regardless of their size, then it follows that $z_- \propto R_1^2$. The detailed relationship, including the zeta potential dependence, is discussed in Appendix C.1.

Noting the experimental uncertainty in ψ_2, and given its variation between the three latexes of differing size, varying this parameter by ± 5 mV leads to $\sim 15\%$ variation in both the D_E/D_a ratio (equation (C.1.7) in Appendix C.1) and the predicted latex front position.

Finally, predictions (black line) for the HOOC-PGMA-PTFEMA nanoparticle experiment shown in Fig. 3b are compared with the experimental data (black data points) shown in Fig. 4b. Theory overpredicts the upwards motion after three days by a factor of approximately four. This is in part because we have assumed an infinitely dilute solution with no hydrodynamic hindrance [5]. Moreover, this suggests that future experiments should focus on validation of the D_a formula for ions of differing size.

5. Conclusions

Existing electrolyte-driven diffusiophoresis theory has been extended for the case where $|z_-| \gg z_+$ and solved numerically to predict latex motion within a nanoparticle concentration gradient for a range of z_- values. This extends the work of Wilson *et al.* [7].

Experimental evidence for this novel diffusiophoretic motion has been obtained using a Hele-Shaw cell, which enables motion of the latex concentration front down the nanoparticle concentration gradient to be observed with good reproducibility. The evolution of the latex front position caused by the nanoparticles and their corresponding counterions is qualitatively consistent with diffusiophoretic theory. This motion is arrested by added salt, which is consistent with the theoretical prediction that $U_E \propto 1/c_{s,total}$. This theory predicts a magnitude of motion that is strongly dependent on z_-. In future studies, this aspect will be examined by using a series of HOOC-PGMA-PTFEMA nanoparticles of varying size (and hence z_-).

Importantly, we demonstrate for the first time that salt-driven diffusiophoresis can occur even if one of the two ions is a nanoparticle. Thus such motion should be considered whenever charged colloids are stabilised by counterions under low or zero salt conditions. Moreover, if other types of diffusiophoresis are to be investigated for such colloids, it follows that high salt concentrations would be required to ensure that salt-driven diffusiophoresis was negligible.

Our observation of nanoparticle-driven diffusiophoresis via an electrostatic mechanism suggests that prior studies of diffusiophoresis in binary mixtures of particles should be re-examined. One example is our previous paper [5], where the magnitude of the diffusiophoretic flux via a geometric argument was not sufficient to explain the observed motion. This electrostatic mechanism provides a physical basis for the observed flux.

CRediT authorship contribution statement

Clare R. Rees-Zimmerman: Conceptualization, Methodology, Formal analysis, Investigation, Writing – original draft. **Derek H.H. Chan:** Methodology, Investigation. **Steven P. Armes:** Methodology, Investigation, Writing – review & editing, Supervision, Funding acquisition. **Alexander F. Routh:** Conceptualization, Methodology, Formal analysis, Investigation, Writing – review & editing, Supervision, Project administration, Funding acquisition.

Declaration of Competing Interest

The authors declare that they have no known competing financial interests or personal relationships that could have appeared to influence the work reported in this paper.

Data availability

Data will be made available on request.

Acknowledgements

CRRZ's work was funded by an Oppenheimer Studentship. The authors thank Lotty Gladstone (Institute for Energy and Environmental Flows, University of Cambridge) for help with the experimental set-up, Andrew Pluck (Institute for Energy and Environmental Flows, University of Cambridge) for making the Hele-Shaw cell, and Daan Frenkel (Department of Chemistry, University of Cambridge) for very helpful discussions. The latex particles were kindly synthesised by Dr. N. Ballard at the University of the Basque Country, Spain. DHHC was supported by an Industrial CASE PhD studentship provided by Syngenta. SPA acknowledges a four-year EPSRC Established Career Particle Technology Fellowship (EP/R003009).

Appendix A. Supplementary data

Supplementary data to this article can be found online at https://doi.org/10.1016/j.jcis.2023.06.115.

References

[1] J.L. Anderson, Colloid transport by interfacial forces, Ann. Rev. Fluid Mech. 21 (1989) 61–99.
[2] D.C. Prieve, J.L. Anderson, J.P. Ebel, M.E. Lowell, Motion of a particle generated by chemical gradients. Part 2. Electrolytes, J. Fluid Mech. 148 (1984) 248–269.
[3] D. Velegol, A. Garg, R. Guha, A. Kar, M. Kumar, Origins of concentration gradients for diffusiophoresis, Soft Matter 12 (2016) 4686–4703.
[4] N. Singh, G.T. Vladisavljević, F. Nadal, C. Cottin-Bizonne, C. Pirat, G. Bolognesi, Enhanced accumulation of colloidal particles in microgrooved channels via diffusiophoresis and steady-state electrolyte flows, Langmuir 38 (46) (2022) 14053–14062.
[5] C.R. Rees-Zimmerman, A.F. Routh, Stratification in drying films: a diffusion–diffusiophoresis model, J. Fluid Mech. 928 (2021) A15.
[6] J.P. Ebel, J.L. Anderson, D.C. Prieve, Diffusiophoresis of latex particles in electrolyte gradients, Langmuir 4 (2) (1988) 396–406.
[7] J.L. Wilson, S. Shim, Y.E. Yu, A. Gupta, H.A. Stone, Diffusiophoresis in multivalent electrolytes, Langmuir 36 (2020) 7014–7020.
[8] B. Akpinar, L.A. Fielding, V.J. Cunningham, Y. Ning, O.O. Mykhaylyk, P.W. Fowler, S.P. Armes, Determining the effective density and stabilizer layer thickness of sterically stabilized nanoparticles, Macromolecules 49 (14) (2016) 5160–5171.
[9] J. Hierrezuelo, A. Sadeghpour, I. Szilagyi, A. Vaccaro, M. Borkovec, Electrostatic stabilization of charged colloidal particles with adsorbed polyelectrolytes of opposite charge, Langmuir 26 (19) (2010) 15109–15111.
[10] G. Fritz, V. Schädler, N. Willenbacher, N.J. Wagner, Electrosteric stabilization of colloidal dispersions, Langmuir 18 (16) (2002) 6381–6390.
[11] Grace, LUDOX® Colloidal Silica - Catalyst Applications, Grace & Co.-Conn, Columbia, 2020.
[12] J.-L. Trompette, J.-F. Lahitte, Influence of the counterion nature on the stability sequence of hydrophobic latex particles, J. Phys. Chem. B 123 (17) (2019) 3859–3865.
[13] S. Shin, E. Um, B. Sabass, J.T. Ault, M. Rahimi, P.B. Warren, H.A. Stone, Size-dependent control of colloid transport via solute gradients in dead-end channels, PNAS 113 (2) (2015) 257–261.

[14] A. Gupta, S. Shim, H.A. Stone, Diffusiophoresis: from dilute to concentrated electrolytes, Soft Matter 16 (2020) 6975–6984.
[15] C. Mauger, R. Volk, N. Machicoane, M. Bourgoin, C. Cottin-Bizonne, C. Ybert, F. Raynal, Diffusiophoresis at the macroscale, Phys. Rev. Fluids 1 (2016), 034001.
[16] P.G. Saffman, Viscous fingering in Hele-Shaw cells, J. Fluid Mech. 173 (1986) 73–94.
[17] H.E. Huppert, A.W. Woods, Gravity-driven flows in porous layers, J. Fluid Mech. 292 (1995) 55–69.
[18] T. ul Islam, P.S. Gandhi, Viscous fingering in multiport Hele Shaw cell for controlled shaping of fluids, Sci. Rep. 7 (2017) 16602.
[19] D.W. van Krevelen. Properties of polymers, 3rd edition, Elsevier, Amsterdam, Lausanne, New York, Oxford, Singapore, Shannon, and Tokyo, 1997.
[20] W.J. Lechnick, J.A. Shaeiwitz, Measurement of diffusiophoresis in liquids, J. Colloid Interface Sci. 102 (1984) 71.
[21] J.L. Keddie, A.F. Routh, An introduction to latex and the principles of colloidal stability. Fundamentals of latex film formation, Springer Laboratory. Springer, Dordrecht, 2010.
[22] J.L. Anderson, D.C. Prieve, Diffusiophoresis: migration of colloidal particles in gradients of solute concentration, Sep. Purif. Methods 13 (1) (1984) 67–103.
[23] M. Kaasalainen, V. Aseyev, E. von Haartman, D.S. Karaman, E. Mäkilä, H. Tenhu, J. Rosenholm, J. Salonen, Size, stability, and porosity of mesoporous nanoparticles characterized with light scattering, Nanoscale Res. Lett. 12 (2017) 74.
[24] B.M. Alessio, S. Shim, A. Gupta, H.A. Stone, Diffusioosmosis-driven dispersion of colloids: A Taylor dispersion analysis with experimental validation, J. Fluid Mech. 942 (2022) A23.
[25] E.J. List, A two-dimensional sink in a density-stratified porous medium, J. Fluid Mech. 33 (3) (1968) 529–643.
[26] Q. Cao, T. Heil, B. Kumru, M. Antonietti, B.V.K.J. Schmidt, Visible-light induced emulsion photopolymerization with carbon nitride as a stabilizer and photoinitiator, Polym. Chem. 10 (2019) 5315–5323.
[27] D.C. Prieve, S.M. Malone, A.S. Khair, R.F. Stout, M.Y. Kanj, Diffusiophoresis of charged colloidal particles in the limit of very high salinity, Proc. Natl. Acad. Sci. U. S. A. 116 (37) (2019) 18257–18262.
[28] S. Shim, J.K. Nunes, G. Chen, H.A. Stone, Diffusiophoresis in the presence of a pH gradient, Phys. Rev. Fluids 7 (2022), 110513.